Springer

KSME

Journal of Mechanical Science and Technology 28 (12) (2014) 4815~4831
www.springerlink.com/content/1738-494x
DOI 10.1007/s12206-014-1102-6

Efficiency improvement of the highly accelerated life testing system by using multiple hammers †

Yeong-Shu Chen* and Le Hong Chuong

Department of Mechanical Engineering, Yuan Ze University, Chungli, Taiwan

(Manuscript Received March 5, 2014; Revised July 17, 2014; Accepted August 19, 2014)

Abstract

Highly accelerated life testing (HALT) is a critical method that combines thermal loadings and a series of vibration step stresses in testing the reliability of electronic products. HALT typically utilizes multiple hammers as the driving force of vibration excitations. In this study, we investigated an existing HALT system and the improved design of the hammer system. We also examined the responses of each table to a variety of effects, such as different combinations of hammers and variations in the impact force angles from the hammers to the table. The investigation begins with a theoretical analysis of the forces of impact exerted by the hammers on the table of the HALT system. Thereafter, ANSYS Workbench software is used to build the simulation model that will verify the accuracy of the theoretical results. Finally, the accelerations of the table in an actual HALT system are measured and analyzed for comparison with the foregoing results.

Keywords: HALT; Hammer; Highly accelerated life testing; Impact; Shock response spectrum

1. Introduction

Highly accelerated life testing (HALT) is extensively utilized in environmental stress screening to ensure the reliability of electronic systems. HALT is an effective tool employed during the product development period by triggering failure modes induced by potential design weaknesses. These weaknesses can be diagnosed and corrected before the product is launched for mass production. Identifying the weakest points in a system or product enables design improvements to increase the overall reliability of the product. Failure at the weakest points in a system leads to system breakdown in the field several months or years after the release of the product.

During the HALT processes for general products, various stress levels, such as those caused by temperature, vibration, pressure, humidity, and radiation, alone or combined, are tested to assess the product life cycle. However, the HALT machine generally used for testing the current consumer electronic products typically includes only different levels of "temperature and vibration" stresses. Basically, the objectives of the HALT system are to determine multiple failure modes and root causes, determine functional operating limits, determine functional destruct limits, and focus on thermal as well as vibration stresses (separately at first and then combined). Under this type of test, the operating limit is defined as the stress level prior to where a failure is identified, but the functionality of the unit under test is recovered when the stress is reduced. By contrast, the destruct limit indicates the stress level where a failure is identified and the functionality of the unit under test is not recovered when the stress is reduced. HALT was developed specifically for solid-state electronics, but can be applied to any product with the correct equipment. The purpose of the HALT system is most effectively met by testing at the lowest possible subassembly. Fig. 1 shows a typical HALT machine with its test chamber and driving hammers mounted under the table.

Vibration step stress test is one of the commonly used HALT test procedures. The goal in using this method is to identify the vibration-related failures by mechanical fatigue testing of the device such that its weakest portions will fail quickly. Fig. 2 shows a typical step acceleration input to the HALT machine. The vibration step increment is typically 5 Grms (the root-mean-square acceleration in terms of gravity). The dwell time at each level is at least 10 min. A full functional test is conducted at the end of the dwell. Thereafter, the vibration stress increases again and the dwell is repeated. Generally, once the operating limit is determined, vibration step stressing continues beyond the operating limit to the destruct limit.

Vibration exertions in the HALT system originate from four basic sources, namely, (1) electromagnetic shaker, (2) hydrau-

*Corresponding author. Tel.: +886 3 4638800, Ext.2473, Fax.: +886 3 4558013
E-mail address: yschen@saturn.yzu.edu.tw
† Recommended by Editor Yeon June Kang

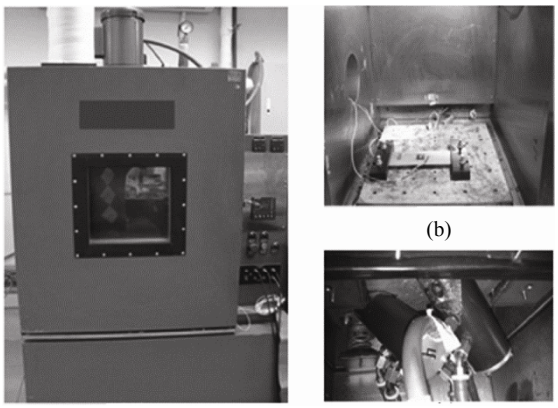

(a) (b) (c)

Fig. 1. (a) Typical HALT machine; (b) test chamber; (c) driving hammer.

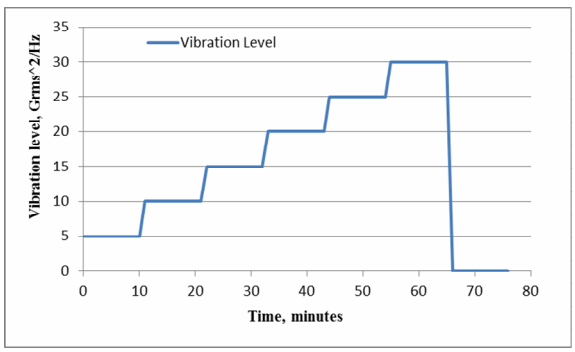

Fig. 2. Example of a vibration step stress test.

lic shaker, (3) multiple pneumatic hammers, and (4) electromagnetic shaker combined with a skewed fixture. The first two sources are typically utilized in products that undergo a uniaxial vibration testing. Multiaxial testing is generally conducted for the last two sources in the reliability enhancement testing. Although most HALT systems utilize multiple pneumatic hammers to drive the table, this method has many disadvantages, such as poor table uniformity, uncontrollable frequency spectrum, small amount of low-frequency energy, and minimal displacement. The test loading condition is significantly different from the actual conditions in which the products operate [1-3]. Liu reported that, among these four sources of vibration, only the electromagnetic shaker combined with a skewed fixture (such as that developed by the author) can produce triaxial vibrations simultaneously [4, 5]. Subsequently, Li et al. [6] developed a more concrete design of the skewed fixture.

Knowing how a table moves under the impact of these hammers can help researchers make improved choices when testing products. In a real-world testing conducted by the authors by controlling the number of acting hammers, they observed that using more hammers does not necessarily generate more displacement of the table. Moreover, using more hammers and manipulating different combinations of them can make the test unit move freely (under the condition of no fixture) with specific patterns on the table. With the development in the miniaturization of electromagnetic shakers into electromagnetic hammers (also called electrodynamic or ED hammer), ED hammers can now be used in the HALT system. In addition to being more efficient than pneumatic hammers, ED hammers can control the individual impact frequency and force, as well as produce shocks at low frequencies [7].

Installing hammers on a testing table can result in various motion combinations. This study aims to analyze the motion of a table when subjected to the impact of various hammer combinations. Based on the results, the performance of the HALT system can be optimized.

2. HALT system model

A typical HALT system consists of a table with driving hammers beneath it. Four hammers, numbered I, II, III, and IV, are installed in the system analyzed in this study. The response of the table is of interest because it can reflect many different excitation patterns on the test specimen. Therefore, this study examines the response of the table to forces induced by the use of either an individual hammer or multiple hammers simultaneously.

2.1 Theoretical model

The HALT system considered in this study consists of a flat table mounted on a set of four springs and four hammers mounted under the table at different orientations, as shown in Fig. 3. The force and frequency of the impact from the hammers are triggered by a controller system.

The first part of the study focuses on the response of the table (i.e., displacement, acceleration, and force) to the various types of impact by the hammers (e.g., the impact of only one hammer or of multiple hammers simultaneously). The initial theoretical force analyses indicate that the forces of impact from the hammers are redistributed equivalently at each of the springs. This finding is the fundamental measure in handling hammer forces throughout the study.

Fig. 4 shows a coordinate system (*OXYZ*) with origin *O* located at the center of the table. The *OXY* plane coincides with the plane of the table. The springs are equidistant from one another in a circle (*O*, *R*) (i.e., the circle centered at *O* with radius *R*). Similarly, the four hammers are attached alternately to the springs and lie on a circle (*O*, *r*). The hammers are installed at an angle α inclined to the plane of the table such that the forces exerted on the table are also inclined at angle α to the *OXY* plane.

2.2 Action of a single hammer

We assumed that Hammer I exerts force $\vec{H}(t)$ instantaneously on the table, as indicated in Fig. 5(a). This force can be separated into three component forces, that is, $\vec{H}_X, \vec{H}_Y, \vec{H}_Z$,

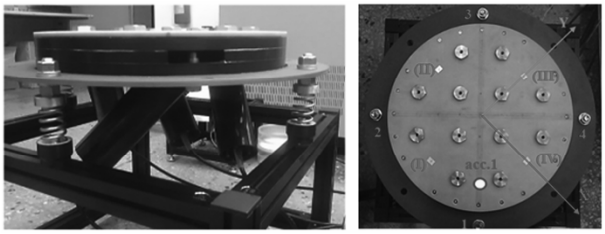

Fig. 3. Construction of an ED hammer system with its table.

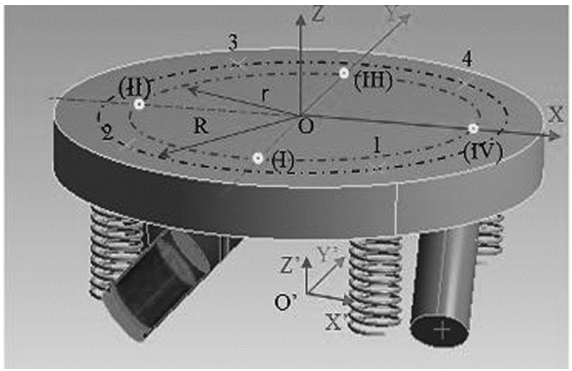

Fig. 4. Coordinate systems defined in the hammer system.

along three coordinate directions, expressed as follows:

$$\vec{H}(t)=\vec{H}_X(t)+\vec{H}_Y(t)+\vec{H}_Z(t).$$

The magnitudes of each of the force components are expressed as follows:

$$H_Z(t)=H(t)\sin(\alpha),$$
$$H_X(t)=H(t)\cos(\alpha)\cos(\beta),$$
$$H_Y(t)=H(t)\cos(\alpha)\sin(\beta),$$

where α is the incline angle of force $\vec{H}(t)$ to the plane of the table (i.e., plane *OXY*) applied by each of the hammers and β is the swing angle between $\vec{H}'(t)$ (i.e., the projection of force $\vec{H}(t)$ onto the *OXY* plane; the magnitude of $\left|\vec{H}'(t)\right|=H(t)\cos(\alpha)$) and the *X*-axis.

We replaced each component of the force $\vec{H}(t)$ of the hammer with the forces acting at the springs on the table to simplify the analysis of the displacement of the table. The force component typically generates two types of motion on the table. One type is a vertical motion along the *Z*-direction. The other type is a rotational motion around the *X*-axis. Following the principle of the equilibrium of rigid bodies [8-10], this force can be replaced by the four equivalent forces on the springs, $\left(\overrightarrow{S^iM^X}\right)_Z$, $i=1$ to 4 , that represent the numbers of springs at the four locations and their directions as shown in Fig. 5(b). For example, $\left(\overrightarrow{S^1M^X}\right)_Z$ is the force along the *Z*-axis on Spring 1 (i.e., S1), which generates a moment (resulting from force $\vec{H}_Z$) with respect to the *X*-axis (i.e., M^X). Thus,

$$\begin{cases}\left(\overrightarrow{S^1M^X}\right)_Z+\left(\overrightarrow{S^2M^X}\right)_Z+\left(\overrightarrow{S^3M^X}\right)_Z+\left(\overrightarrow{S^4M^X}\right)_Z \\ \qquad =\sum_{i=1}^{4}\left(\overrightarrow{S^iM^X}\right)_Z=\vec{H}_Z \\ \sum_{i=1}^{4}\left(\overrightarrow{S^iM^X}\right)_Z a=\vec{H}_Z r\end{cases}, \tag{1}$$

where r is the distance of the force component $\vec{H}_Z$ of the hammer to the center of table *O* and a is the distance of the *i*-th spring from the *X*-axis. Given that the springs are equidistant to one another in circle (*O*, *R*), as shown in Fig. 5(a), $a=R(\sin 45°)=\left(\sqrt{2}/2\right)R$. Solving Eq. (1) results in

$$\begin{cases}\left(S^1M^X\right)_Z=\left(S^2M^X\right)_Z=\dfrac{\sqrt{2r}+R}{4R}H_Z\uparrow \\ \left(S^3M^X\right)_Z=\left(S^4M^X\right)_Z=\dfrac{\sqrt{2r}-R}{4R}H_Z\downarrow\end{cases}, \tag{2}$$

where ↑ indicates the forces pointing to the positive direction along the *Z*-axis, whereas ↓ indicates the forces pointing to the negative direction along the *Z*-axis.

Similarly, in Fig. 5(a), force component $\vec{H}_Y$ can move the table along the *Y*-axis and can be replaced by the four translational forces located at each of the springs in the direction of the *Y*-axis. For example, as shown in Fig. 5(b), $\left(S^2T\right)_Y$ is the force on Spring 2 (i.e., S2) that can generate a translational movement (i.e., *T*) along the *Y*-axis, expressed as follows:

$$\begin{cases}\sum_{i=1}^{4}\left(\overrightarrow{S^iT}\right)_Y=\vec{H}_Y=\vec{H}_{OY} \\ \sum_{i=1}^{4}\left(\overrightarrow{S^iT}\right)_Y a=\vec{M}_{OZ}=0\end{cases}. \tag{3}$$

Therefore,

$$\left(S^1T\right)_Y=\left(S^2T\right)_Y=\left(S^3T\right)_Y=\left(S^4T\right)_Y=\frac{H_Y}{4}\uparrow, \tag{4}$$

where ↑ indicates the forces pointing to the positive direction along the *Y*-axis, whereas ↓ indicates the forces pointing to the negative direction along the *Y*-axis.

Force component $\vec{H}_X$ generates two types of motion on the table. One type is a linear motion along the *X*-direction. The other type is a rotational motion in the *Z*-direction. The motion along the *X*-direction can be replaced by the four translational forces located at the four springs, as shown in Fig. 5(b), and expressed as follows:

$$\begin{cases} \sum_{i=1}^{4}\left(\overrightarrow{S^iT}\right)_X = \vec{H}_X = \vec{H}_{OX} \\ \sum_{i=1}^{4}\left(\overrightarrow{S^iT}\right)_X a = 0 \end{cases}. \tag{5}$$

Eq. (5) produces the following equation:

$$\begin{aligned} \left(S^1T\right)_X = \left(S^2T\right)_X = \left(S^3T\right)_X = \left(S^4T\right)_X \\ = \frac{\sqrt{2}H_X r}{4R} \rightarrow, \end{aligned} \tag{6}$$

where → shows the forces pointing to the positive direction along the *X*-axis, whereas ← indicates the forces pointing to the negative direction along the X-axis.

The moment component can rotate the table in the *Z*-axis and can be replaced by the four tangential forces that lie on circle (*O*, *R*) and at each of the springs, as indicated in Fig. 5(b) and expressed as follows:

$$\sum_{i=1}^{4}\left(\overrightarrow{S^iM^Z}\right)R = \vec{H}_X r = \vec{M}_{OZ}. \tag{7}$$

Eq. (7) results in the following equation:

$$\left(S^1M^Z\right) = \left(S^2M^Z\right) = \left(S^3M^Z\right) = \left(S^4M^Z\right) = \frac{H_X r}{4R}. \tag{8}$$

The force of the spring that generates the moment, $\left(\overrightarrow{S^iM^Z}\right)$, can be separated into two component forces on the *OXY* plane along the *X*- and *Y*-axes. Fig. 5(b) indicates that

$$\left(\overrightarrow{S^iM^Z}\right)_X + \left(\overrightarrow{S^iM^Z}\right)_Y = \left(\overrightarrow{S^iM^Z}\right) \tag{9}$$

or

$$\begin{aligned} \left(S^iM^Z\right)_X = \left(S^iM^Z\right)_Y = \frac{H_X r}{4R}\sin(45°) \\ = \frac{\sqrt{2}H_X r}{8R}. \end{aligned} \tag{10}$$

The foregoing calculations for the analysis of the effects of the force from a single hammer on the table indicate that this hammer force with its equivalent components can be replaced by a series of forces (such as those causing translation and rotation) along each of the axes of the coordinate system (*OXYZ*). $\overrightarrow{S^i}_X$ is the force on spring *i* along the *X*-direction, $\overrightarrow{S^i}_Y$ is the force on spring *i* along the *Y*-direction, and $\overrightarrow{S^i}_Z$ is the force on spring *i* along the *Z*-direction, calculated as follows:

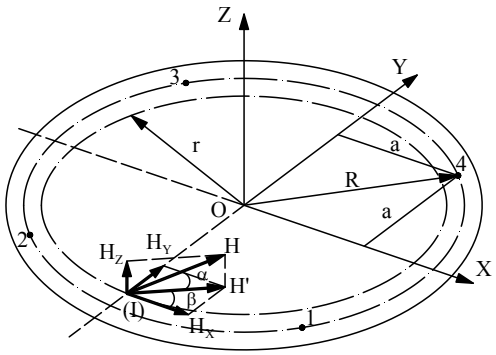

(a)

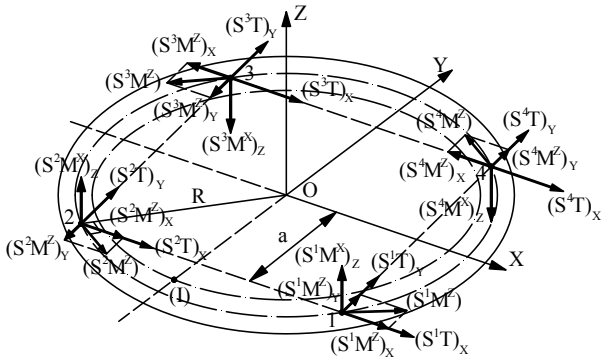

(b)

Fig. 5. Equivalent force system on the springs.

$$\begin{cases} \overrightarrow{S^i}_X = \left(\overrightarrow{S^iT}\right)_X + \left(\overrightarrow{S^iM^Z}\right)_X \\ \overrightarrow{S^i}_Y = \left(\overrightarrow{S^iT}\right)_Y + \left(\overrightarrow{S^iM^Z}\right)_Y \\ \overrightarrow{S^i}_Z = \left(\overrightarrow{S^iM^X}\right)_Z \end{cases}, \quad i = 1 \text{ to } 4. \tag{11}$$

As shown in Eq. (11), the force of Spring 1 along the *X*-direction, $\overrightarrow{S^1}_X$, is the result of two forces, namely, a force that generates translation, $\left(\overrightarrow{S^1T}\right)_X$, and another force that generates a rotational moment, $\left(\overrightarrow{S^1M^Z}\right)_X$. The corresponding values of these forces are provided in Table 1.

The aforementioned analyses are summarized as follows:

(1) When a table is impacted by the other single hammers (e.g., Hammer II, III, or IV), the motion of the table can be analyzed in a manner similar to the analysis of Hammer I, except that the geometric relationship between the hammer and springs must be considered. For example, the force components on Spring 1 resulting from the impact of Hammer III are exactly similar in magnitude to those on Spring 3 resulting from the impact of Hammer I. However, they point in opposite directions, except for the forces in the *Z*-direction, as shown in Fig. 6(a). Moreover, the force components on Spring 1 resulting from the impact of Hammer II are exactly similar

Table 1. The total force of each spring along the three axes.

Spring \ Axis	X	Y	Z
1	$\frac{2R+\sqrt{2}r}{8R}H\cos(\alpha)\cos(\beta)$	$\frac{2R\sin(\beta)+\sqrt{2}r\cos(\beta)}{8R}H\cos(\alpha)$	$\frac{\sqrt{2}r+R}{4R}H\sin(\alpha)$
2	$\frac{2R+\sqrt{2}r}{8R}H\cos(\alpha)\cos(\beta)$	$\frac{2R\sin(\beta)-\sqrt{2}r\cos(\beta)}{8R}H\cos(\alpha)$	$\frac{\sqrt{2}r+R}{4R}H\sin(\alpha)$
3	$\frac{2R-\sqrt{2}r}{8R}H\cos(\alpha)\cos(\beta)$	$\frac{2R\sin(\beta)-\sqrt{2}r\cos(\beta)}{8R}H\cos(\alpha)$	$\frac{\sqrt{2}r-R}{4R}H\sin(\alpha)$
4	$\frac{2R-\sqrt{2}r}{8R}H\cos(\alpha)\cos(\beta)$	$\frac{2R\sin(\beta)+\sqrt{2}r\cos(\beta)}{8R}H\cos(\alpha)$	$\frac{\sqrt{2}r-R}{4R}H\sin(\alpha)$

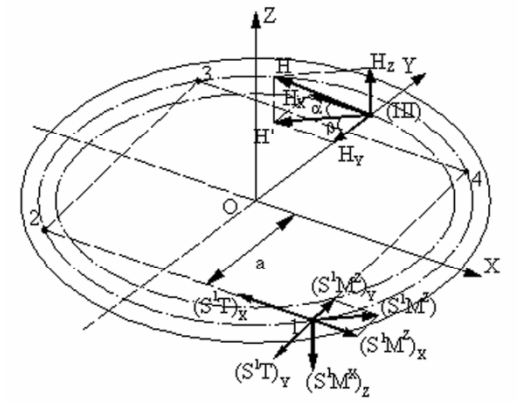

(a) Impact by Hammer III

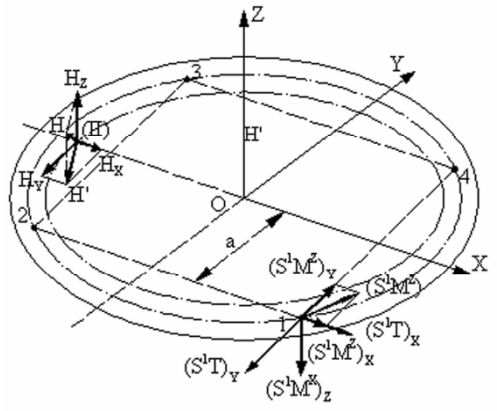

(b) Impact by Hammer II

Fig. 6. Force components at Spring 1 caused by the impact of a single hammer.

to those on Spring 4 resulting from the impact of Hammer I. However, they point in opposite directions, except for the forces in the *Z*-direction, as shown in Fig. 6(b).

(2) Given a change in the direction of the force of the impact (i.e., variation in angles, namely, incline angle α and swing angle β) resulting from the mounting of the hammers to the table, all force components on the spring also change.

(3) The appropriate hammer location, contact angle of the hammer, and combination of hammers must be selected to achieve the best output of the table.

Table 2. Total forces on each of the springs along the three axes in using Hammer I for the case with fixed angles of $\alpha = 45°$ and $\beta = 0°$.

Spring \ Axis	X	Y	Z
1	$\frac{\sqrt{2}R+r}{8R}H\rightarrow$	$\frac{r}{8R}H\nearrow$	$\frac{2r+\sqrt{2}R}{8R}H\uparrow$
2	$\frac{\sqrt{2}R+r}{8R}H\rightarrow$	$\frac{r}{8R}H\swarrow$	$\frac{2r+\sqrt{2}R}{8R}H\uparrow$
3	$\frac{\sqrt{2}R-r}{8R}H\rightarrow$	$\frac{r}{8R}H\swarrow$	$\frac{2r-\sqrt{2}R}{8R}H\downarrow$
4	$\frac{\sqrt{2}R-r}{8R}H\rightarrow$	$\frac{r}{8R}H\nearrow$	$\frac{2r-\sqrt{2}R}{8R}H\downarrow$

In real-life applications, the hammers in the HALT systems are usually fixed by the manufacturer. Changing their positions or contact angle (generally, $\alpha = 45°$) is impossible. The projected force of the impact of each hammer on the *OXY* plane is tangential to circle (O, r) ($\beta = 0°$). We consider a type of fixed (special) case using Hammer I with $\alpha = 45°$ and $\beta = 0°$. By substituting these numbers into Table 1, the component forces are rewritten similarly, as shown in Table 2. The arrowheads for each of the forces indicate the directions they point to.

Understanding the effects and relationships of these parameters is difficult because of the many parameters included in this table. Thus, all of these parameters were simplified using new substitutions of symbols by letting

$$k = \frac{R}{r} = const \geq 1, \quad D_1 = \frac{r}{8R}H, \\ E_1 = \frac{\sqrt{2}R}{8R}H = \left(k\sqrt{2}\right)D_1 \Leftrightarrow E_1 > D_1 \tag{12}$$

and

Table 3. Spring forces in each of the three axes in using Hammer I, as represented by the shortened parameters.

Axis / Spring	X	Y	Z
1	$bD_1 \rightarrow$	$D_1 \nearrow$	$dD_1 \uparrow$
2	$bD_1 \rightarrow$	$D_1 \swarrow$	$dD_1 \uparrow$
3	$cD_1 \rightarrow$	$D_1 \swarrow$	$eD_1 \downarrow$
4	$cD_1 \rightarrow$	$D_1 \nearrow$	$eD_1 \downarrow$

$$b = k\sqrt{2}+1, \quad c = k\sqrt{2}-1, \quad d = k\sqrt{2}+2, \\ e = 2-k\sqrt{2} \quad \Leftrightarrow d > b > c > e \geq 0. \tag{13}$$

The formulas in Table 2 are shown again in Table 3 with these substitutions. Thus, the advantage of using these new symbols can be addressed. For example, after checking the forces at Springs 1 and 2 under the action of a single hammer (Hammer I), we observed that the force magnitudes in the *X*-direction are smaller than those in the *Z*-direction (given that $d > b$). In the same table, the force in the *Y*-direction is merely a factor of the difference between *b* and *d* in the *X*- and *Z*-directions, respectively. Similarly, after checking the column under the *X*-direction, we observed that the forces in Springs 1 and 2 are exactly similar. The same situation was observed for the forces in Springs 3 and 4. However, the forces in Springs 3 and 4 have smaller values compared with those in Springs 1 and 2 (given that $b > c$). All of these forces under column *X* pointed to the same direction.

2.3 Analysis of table displacement

The motion of the table when impacted by hammers can be analyzed by calculating the displacement at each of the four springs caused by the force components discussed previously.

Fig. 5 shows that, with regard to the motion of the table when impacted by Hammer I, the force of the impact can be replaced with the resulting force components at all four springs. Therefore, the motion of the table can be determined by calculating the displacement of the four springs acted upon by these force components. The analysis in the preceding section indicated that the spring not only was compressed along the *Z*-direction but was also bent in the *X*- and *Y*-directions. $\vec{S^i}_X$, $\vec{S^i}_Y$, and $\vec{S^i}_Z$ are the spring forces expressed in Eq. (11).

The deflection of the spring can be calculated using the following equation:

$$\{S\} = \{k_s\}\{\delta\}, \tag{14}$$

where $\{S\}$ is the force matrix acting on the springs, $\{k_s\}$ is the stiffness matrix of the spring, and $\{\delta\}$ is the deflection of the spring along the three axes.

The components of the deflection of a spring along the three directions can be calculated using the equations in Table 1 and Eq. (11). However, the combined effects of the hammers on deflections along all of the three axes should also be considered.

It is supposed that the bottom of the spring is fixed on a plane, where it attaches to a frame structure to support the entire system. As indicated in Fig. 4, a coordinate system (*O*′-*X*′-*Y*′-*Z*′) is set on this fixed plane, with *O*′*Z*′ pointing in the same direction as *OZ* (*O*′*Z*′ ≡ *OZ*) and *O*′*X*′ being parallel to *OX* (*O*′*X*′//*OX*) and *O*′*Y*′//*OY*. A lateral movement as well as a rotational motion around the $\vec{Y'}$ and *X*′ axes occur because force components $\vec{S^i}_X$ and $\vec{S^i}_Y$ in Fig. 5 act on top of the spring. Meanwhile, the table to which the springs are attached has the same motion as the deflections of the spring. Thus, the final deflection of the table along the $\vec{Z'}$-axis can be determined. Similarly, the force component $\vec{S^i}_Z$ can cause simultaneous deflections along the *Z*′- and *Y*′-axes.

To better describe the effects of the springs, the physical principle for combining multiple springs [11-15] can be utilized to transform the four springs, each with various individual deflections, into one spring located at the center of the table. The stiffness of this transformed single spring along the three axes can be calculated by the following equation:

$$\begin{Bmatrix} (k_t)_X \\ (k_t)_Y \\ (k_t)_Z \end{Bmatrix} = \left\{ f\begin{pmatrix} k_X^i \\ k_Y^i \\ k_Z^i \end{pmatrix} \right\} \quad \text{or} \quad \{k_t\} = \left\{ f\left(k^i\right) \right\}, \tag{15}$$

where $\{k_t\}$ is the matrix of the equivalent total spring stiffness with components in the *X*-, *Y*-, and *Z*-axes designated as $(k_t)_X$, $(k_t)_Y$, and $(k_t)_Z$, respectively. $\left\{ f\left(k^i\right) \right\}$ is a function of the stiffness matrix for each of the original four springs in the three axes (i.e., k_X^i, k_Y^i, and k_Z^i), where *i* represents the number of springs (*i* = 1-4).

As shown in Fig. 7, for the force along the *X*′-axis, force component $\vec{S^i}_X$ (*i* = 1-4) can be replaced by $\vec{F}_X$ at the center of the table. Similarly, force component $\vec{S^i}_Y$ can be replaced by $\vec{F}_Y$ at the center of the table. For example, for the motion of a table impacted by $\vec{F}_X$, the lateral deflection δ_{X1} along the *X*′-axis can be calculated as follows:

$$\delta_{X1} = \frac{F_X}{(k_t)_X}. \tag{16}$$

If the deflection is small, then the change in the length of the spring can be ignored. This lateral deflection causes the longitudinal axis of the spring to rotate at an angle of $\gamma = \arcsin\left(\delta_{X1}/L\right)$, where *L* is the length of the spring that is unchanged (Fig. 7(c)). Similarly, the displacement of the table along the *Z*-axis, that is, δ_{Z1}, at spring locations 2 and 3 (position *A* in Fig. 7(c)) can also be calculated when the table is

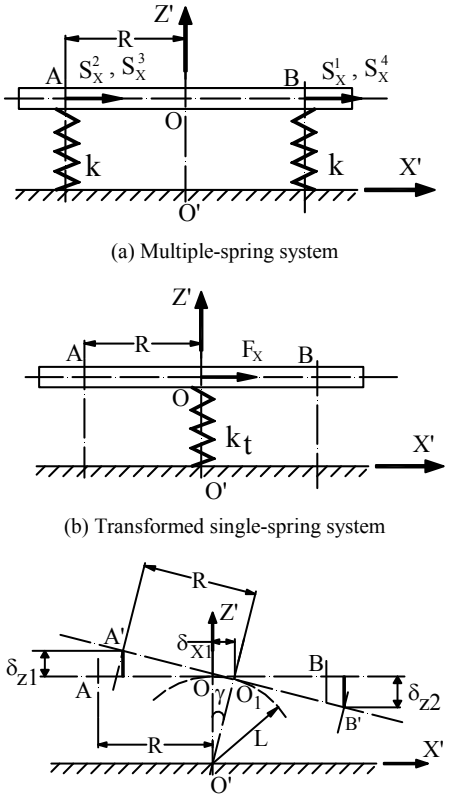

Fig. 7. Transformation of multiple springs into a single spring.

impacted by $\vec{F}_X$. Impact force $\vec{F}_X$ only causes the rotation of the table along the *Y*-axis, as shown in Fig. 7.

Thus, calculating the deflections of general spring positions through the center locations of the springs designated as A and B is easy, as indicated in Fig. 7(c) and the following equation:

$$\begin{cases} \delta_{Z1} = \left[R - L\tan(\gamma)\right]\sin(\gamma) \\ \delta_{Z2} = \left[R + L\tan(\gamma)\right]\sin(\gamma) \end{cases}. \tag{17}$$

In the case that the motion of the table is impacted by Hammer I, the deflections along the *Z*-axis for Springs 2 and 3 (Location A) move upward and the deflections of Springs 1 and 4 (Location B) move downward.

Similarly, when considering the table being impacted by translational force $\vec{F}_Y$, the deflections along the *Z*-axis of Springs 1 and 2 move upward and the deflections of Springs 3 and 4 move downward. Force component $\vec{H}_Z$ along the Z-direction resulting from the impact of Hammer I generate a bending moment around the *X*-axis. The deflections of the four springs along the *Y*-axis are equal to one another.

By combining all of the deflection components along the directions of the three axes for the case of Hammer I in exerting force $\vec{H}(t)$ on a table, we can summarize the deflections of the table at the four springs as follows:

- Deflections along the *X*-direction: $\delta_{1X} = \delta_{2X} > \delta_{3X} = \delta_{4X}$;
- Deflections along the *Y*-direction: $\delta_{1Y} = \delta_{4Y} > \delta_{2Y} = \delta_{3Y}$;
- Deflections along the *Z*-direction: $\delta_{2Z} > \delta_{1Z} > \delta_{3Z} > \delta_{4Z}$.

These analyses show that, when a single hammer acts at different locations, it results in different force components along the three axes at a specific position on the table. When comparing the forces in the last column of Table 3 for the spring forces in the *Z*-axis, we observed that Springs 1 and 2 have exactly the same values. The same observation was obtained for Springs 3 and 4. However, the deflections at each of the spring locations along the *Z*-direction are different, that is, $\delta_{2Z} > \delta_{1Z} > \delta_{3Z} > \delta_{4Z}$, as previously mentioned in the summarized conclusions of the deflections of the table. Moreover, Fig. 7(c) shows that the deflection value at the center of the table (Location "O") is the smallest compared with those on the outer edges of the locations of the four springs.

The entire table plane moves either in a translational or rotational manner because the table is sufficiently rigid. The accelerations at each point on the table depend on the corresponding deflections of that point because acceleration is the second derivative of displacement with respect to time.

2.4 Force impact and spring stiffness

In the HALT systems, the force of the impact from each hammer creates an instantaneous shock on the table. The magnitude and direction of this shock are fully dependent on the force of the impact. The force of this impact results from the motion of the piston inside the hammer housing. As the piston moves up and down in the cylinder, the direction of the impact changes accordingly. This change also causes a change in the direction of the shock pulse on the table.

The stiffness of the spring also affects the motion of the table. As shown in Eq. (16), spring stiffness and the motion of the table are inversely proportional to each other.

3. Table responses when multiple hammers are combined

When the table is impacted by the simultaneous forces of multiple hammers, the total resultant force at a specific spring is not simply the sum of the forces of each individual hammer. The direction of the corresponding forces that act on the same spring must be considered.

Theoretically, the locations and incline angles of the hammers mounted under the table can be changed to obtain the greatest impact. However, in reality, the hammers in HALT systems are usually fixed by the manufacturer. Thus, changing their positions or contact angle is impossible. Fig. 8 shows a typical installation of four equidistant hammers whose top surfaces come in contact with the table by lying on a circular path centered at *O* with radius *r*. In fact, these hammers were installed beneath the table with a contact surface of 45° relative to the table, with the orientation of the hammer pointing at the tangential direction of the circle (*O*, *r*). Thus, the projected force of the impact of each hammer on the *OXY* plane (e.g.,

$H1_X$) is tangential to circle (*O*, *r*), whereas the other projection of impact force points vertically away from the table surface along the *Z*-axis. Then, we consider several cases with the same settings of the hammers, except that the number of hammers used is changed.

The general case in an actual system is that all four hammers simultaneously act with a magnitude similar to their impact forces (i.e., $\left|\overrightarrow{H1}\right| = \left|\overrightarrow{H2}\right| = \left|\overrightarrow{H3}\right| = \left|\overrightarrow{H4}\right| = \left|\overrightarrow{H}\right|$) (Table 4). The magnitudes of the component forces in each of the three axes (i.e., X, Y, and Z) are similar in all spring positions. However, the directions they point to are different. For example, as indicated in column X, the values are all equal to *4D,* and the forces of Springs 1 and 2 point to the right, whereas those of Springs 3 and 4 point to the left. This observation is explained by Eq. (12), where the simplified parameter for a single hammer is designated as $D_1 = (r/8R)H1$. Each hammer has the same force magnitude (i.e., $\left|\overrightarrow{H1}\right| = \left|\overrightarrow{H2}\right| = \left|\overrightarrow{H3}\right| = \left|\overrightarrow{H4}\right| = \left|\overrightarrow{H}\right|$), which provides the total hammer force equal to *4D* (i.e., $D_1 = D_2 = D_3 = D_4 = D$). Similar results are obtained for the Y-axis except for the similarity of both the values and directions of all spring forces on the Z-axis. All forces shown in Table 4 result in the translation of the table along the Z-axis and the rotation around the Z-axis. The HALT test performed in this situation excites the specimen mostly in the Z direction while simultaneously producing minor rotations.

In the case with only three hammers (e.g., Hammers I, III, and IV), the magnitudes of the force components along the Y- and Z-axes at Springs 1 and 4 are larger than those in the previous case with four hammers (Table 5). In other words, the use of all four hammers does not always generate larger forces. The table moves along the Y- and Z-axes and simultaneously rotates around the Z-axis in this case. Accordingly, the specimen is subjected to loadings in these two directions.

The ratios among all force components in the overall exerting force on the table.

Table 6 shows the force value at the spring locations when four hammers are used (Fig. 9). All hammer forces in the figure point to the same direction at angles $\alpha = 45°$ and $\beta = 0°$. The spring force value ratio with different acting directions along the X- and Z-axes is X:Z = 1:1.

In summary, the ratio of spring forces along the three axes (i.e., X:Y:Z) varies when the hammer angles (i.e., incline angle α and swing angle β) in the design of a HALT system is altered. This variation identifies the most efficient position for specimen attachment on a HALT system table.

The preceding cases yield some interesting findings. For example, all forces on the X-direction in each spring location cancel out one another (i.e., Springs 1 and 2 have force *4D*→ and Springs 3 and 4 have force *4D*←). The similar cancellations are also observed in the spring forces on the Y-direction (Table 4). The table still rotates even though all forces are cancelled because of the existing resulting moment. By contrast, the forces in the spring locations in Table 6 indicate that the resulting force is maximized and minimized along certain directions by changing the mounting angles of the hammers. Correspondingly, the forces along the X- and Z-directions are the maximum, whereas the forces along the Y-direction are the minimum (i.e., zero).

Table 4. Force components at all the spring positions when four hammers are used.

Spring \ Axis	X	Y	Z
1	$4D \rightarrow$	$4D \nearrow$	$4E \uparrow$
2	$4D \rightarrow$	$4D \swarrow$	$4E \uparrow$
3	$4D \leftarrow$	$4D \swarrow$	$4E \uparrow$
4	$4D \leftarrow$	$4D \nearrow$	$4E \uparrow$

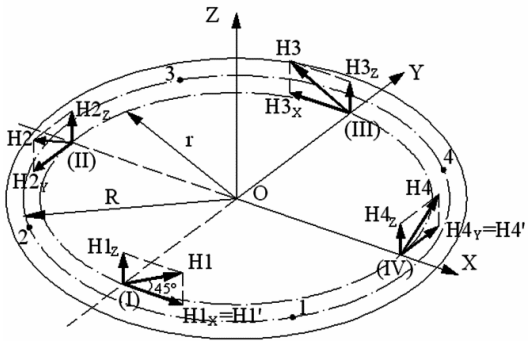

Fig. 8. Forces of impact on the table from each of the four hammers.

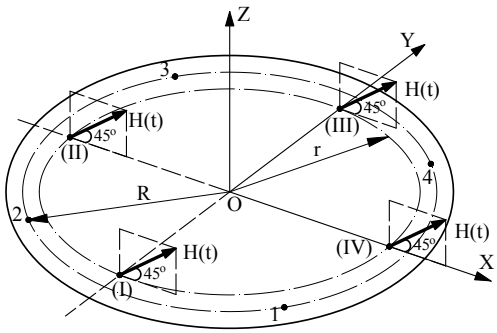

Fig. 9. Forces of impact on the table from each of the four hammers with the same direction.

4. Simulation of a HALT system

The preceding sections have presented the theoretical analysis for the mechanics of a HALT system. The current section describes the commercially available ANSYS Workbench software used to create a HALT model, which evaluates the theoretical model.

The model comprises a flat table mounted on a set of four springs. All springs are fixed on the bottom of the table (Fig. 4). The geometric dimensions of the table and the springs are as follows:

Table 5. Force components at all the spring positions when three hammers (i.e., I, III, and IV) are used.

Spring \ Axis	X	Y	Z
1	$3D \rightarrow$	$3D+E \nearrow$	$3E+2D \uparrow$
2	$3D \rightarrow$	$3D-E \swarrow$	$3E-2D \uparrow$
3	$3D \leftarrow$	$3D-E \swarrow$	$3E-2D \uparrow$
4	$3D \leftarrow$	$3D+E \nearrow$	$3E+2D \uparrow$

Table 6. Forces at each spring location in the case indicated in Fig. 9.

Spring \ Axis	X	Y	Z
1	$4E \rightarrow$	0	$4E \uparrow$
2	$4E \rightarrow$	0	$4E \uparrow$
3	$4E \rightarrow$	0	$4E \uparrow$
4	$4E \rightarrow$	0	$4E \uparrow$

- Table: diameter = 500 mm and thickness = 100 mm.
- Springs: outside diameter (Do) = 50 mm, wire diameter (dw) = 4 mm, number of active coils (n) = 10, and total height = 100 mm.

The hammers and springs are equally spaced on a circle centered at O with a diameter of 200 mm.

The deflections at the four spring positions are respectively shown in Figs. 10(b)-(d) with regard to the assumption that the table is impacted by a single hammer acting at location I. This hammer has exactly the same mounting angles (i.e., $\alpha = 45°$ and $\beta = 0°$) as those used in the current HALT system (Sec. 2). If we suppose that the table and hammers are rigid, then the comparison of the large spring deflections with the corresponding results for the deflections at all springs along the three axes is summarized as follows:

- Among the plots in Fig. 10, the most noteworthy case is that of the deflections along the X-direction. Fig. 10(c) shows that $\delta_{1X} = \delta_{2X} > \delta_{3X} = \delta_{4X}$ and all deflections are positive.
- For the deflections along the Y-direction, $\delta_{1Y} = \delta_{4Y} > \delta_{2Y} = \delta_{3Y}$. The deflections of Springs 1 and 4 are positive, whereas those of Springs 2 and 3 are negative, as shown in Fig. 10(d).
- For the deflections in the Z-direction, $\delta_{2Z} > \delta_{1Z} > \delta_{3Z} > \delta_{4Z}$. The table deflections at Springs 1 and 2 point upward, whereas those at Springs 3 and 4 point downward as shown in Fig. 10(b).

All spring deflections are completely consistent with the explanations from the previous section. Thus, the theoretical model accurately depicts the table response to the hammer impact.

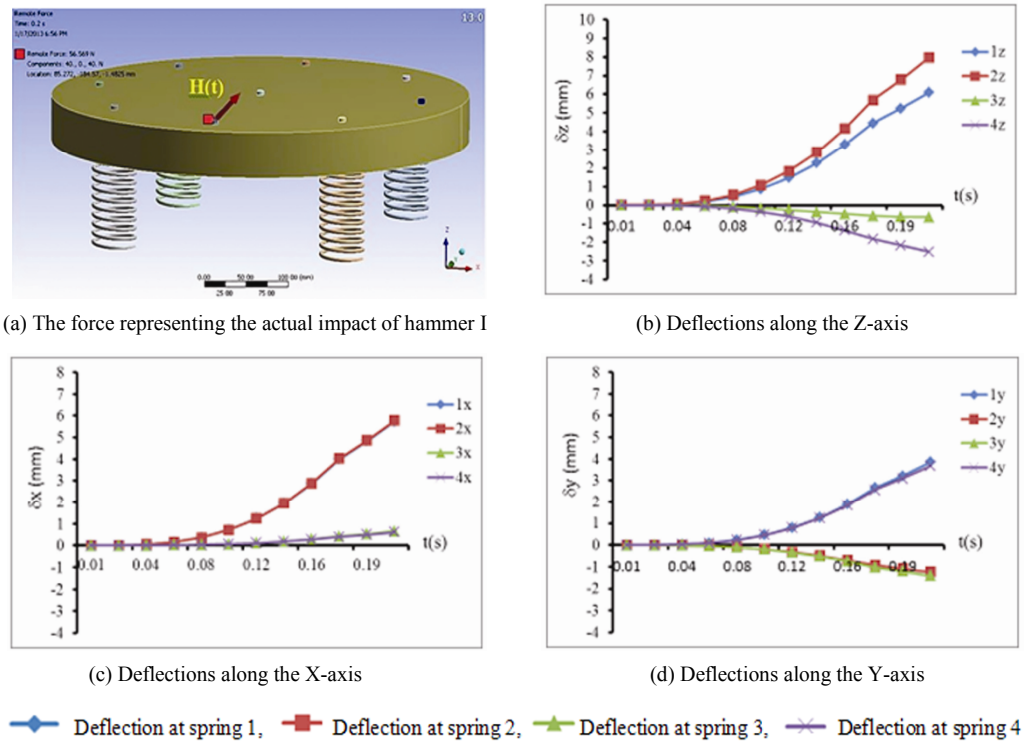

(a) The force representing the actual impact of hammer I

(b) Deflections along the Z-axis

(c) Deflections along the X-axis

(d) Deflections along the Y-axis

Fig. 10. Deflections of the table impacted by $\vec{H}(t)$.

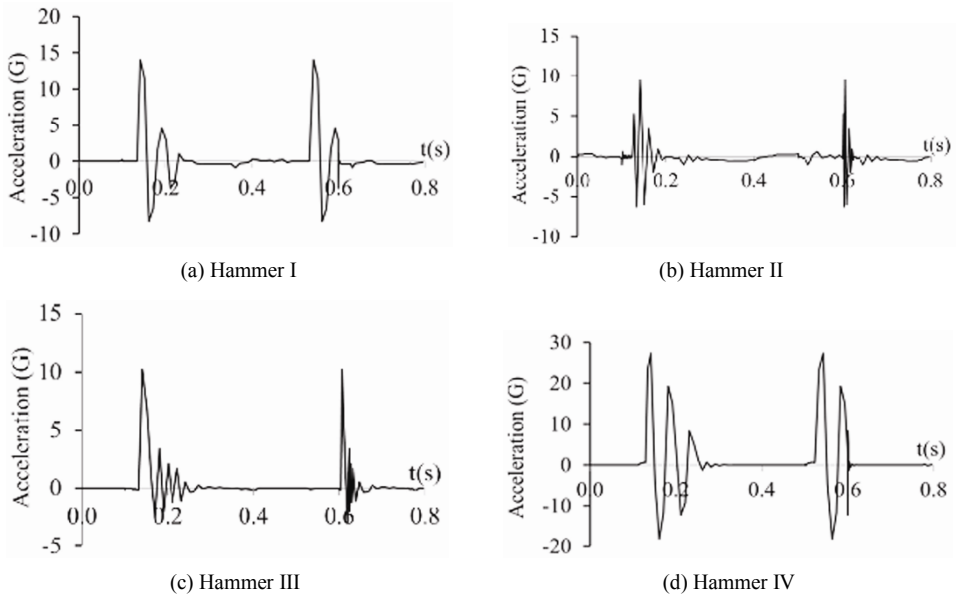

(a) Hammer I (b) Hammer II

(c) Hammer III (d) Hammer IV

Fig. 11. Accelerations along the Z-axis at Spring 1 when acted upon by each single hammer.

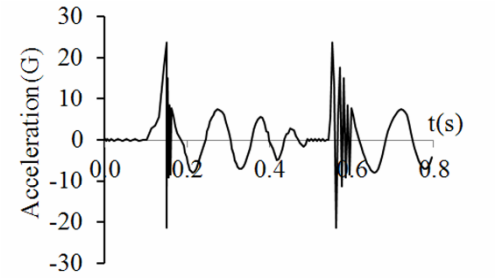

Fig. 12. Table accelerations along the Z-axis at Spring 1 when acted upon by Hammers II and III.

4.1 Response of the table to different impacts (i.e., a single hammer at various locations, multiple hammers, and a change in the hammer angle)

The theoretical analysis shows that the table responds differently at a fixed point when a single hammer acts at different locations. This result is derived by considering four separate cases of a single hammer acting at one of the four hammer positions (i.e., I, II, III, and IV). The HALT system model contains four hammers equidistantly arranged from one another in a circular path around the center of the table (Fig. 4). These hammers come into direct contact with the table. At each moment of impact, the control of the hammer through the piston displacement inputs is identical. The differences in the maximum acceleration for all cases at Spring 1 along the Z-axis are shown in Fig. 11. For example, as shown in Figs. 11(a) and (d), the maximum accelerations are 14.1 and 27.4 G for Hammers I and IV, respectively.

Fig. 12 indicates that the maximum acceleration at Spring 1 is 23.6 G when Hammers II and III impacted the table simultaneously. However, this acceleration does not exceed that of Hammer IV (i.e., 27.4 G) impacting the table, as shown in Fig. 11(d).

The theoretical analysis data also show that the force components on the spring change when the impacting force direction is varied (i.e., angle α or β). These angles depend on the mounting angle of the hammer to the table. Correspondingly, the table motion is changed. The acceleration along the three axes of the table at Spring 1 when Hammer I acts on the table with a swing angle of $\beta = -90°$ is shown in Fig. 13(a). Correspondingly, the projected force of the hammer on the O-XYZ plane is along the negative Y-axis. Therefore, the overall resulting table motion is mainly along the Z- and Y-axes. However, a small oscillating motion occurs along the X-axis because the force applied to the table is asymmetric. Thus, changing the swing angle β of Hammer I also changes the table movements. For example, the maximum acceleration (i.e., 29.3 G) for Hammer I with angle $\beta = -90°$ along the Z-axis becomes 14.1 G with angle $\beta = 0°$ (Fig. 11(a)).

4.2 Hammer stroke and spring stiffness effects on the table response

When the piston moves up and down inside the hammer housing, its movement causes the direction of the acceleration shock pulses to change accordingly. The two following strokes are observed when a table is impacted by a single hammer acting at location I from time period $t = 0$-0.14 s and at the start of the piston movement:

Single-impact stroke: the piston impacts only the anvil at the front end of the hammer. This type of stroke also occurs when a gap exists between the front end of the hammer and the table (i.e., the bottom of the hammer is installed at the frame but its front end does not make contact with the table).

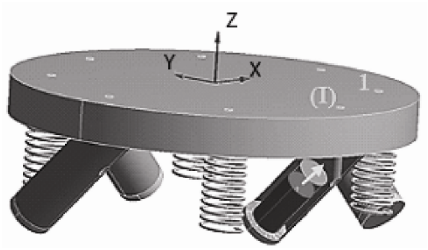

(a) Hammer I with $\beta = -90°$

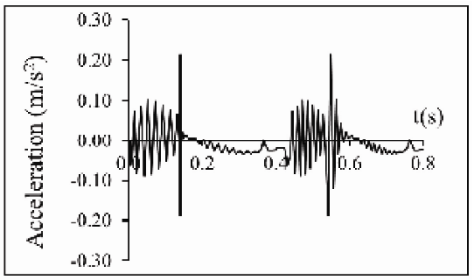

(b) Acceleration along the X-axis

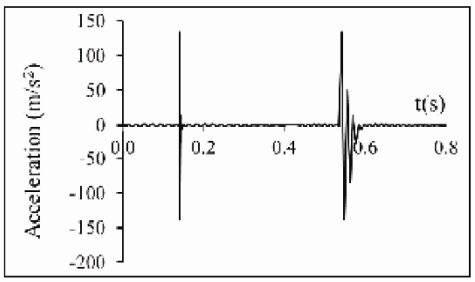

(c) Acceleration along the Y-axis

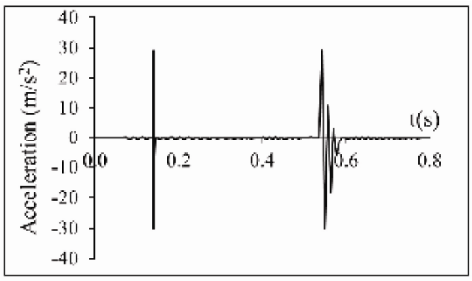

(d) Acceleration along the Z-axis

Fig. 13. Model responses to hammer I with angle $\beta = -90°$.

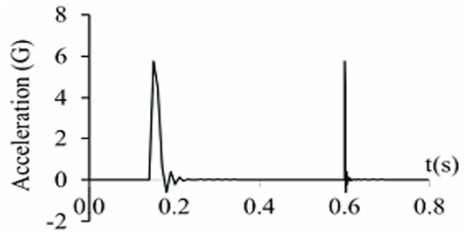

(a) Accelerations of the table along the Z-axis for the single-impact stroke

(b) Acceleration of the table along the Z-axis for the dual-impact stroke

Fig. 14. Effects of piston stroke on the table accelerations.

Dual-impact stroke: the piston impacts both ends of the cylinder.

Figs. 14(a) and (b) shows the table acceleration along the Z-axis at Spring 1. The two plots indicate that the piston hitting the front end of the hammer generates only a unidirectional impact (Fig. 14(a)), whereas the piston hitting both ends of the hammer can result in shock pulse accelerations in both positive and negative directions (Fig. 14(b)).

The magnitude and shape of the time history shock pulse also change when the spring stiffness changes. The table acceleration in response to two different values of spring stiffness is shown in Fig. 15. Fig. 15(b) shows double the spring stiffness of Fig. 15(a). The figures show that a stiffer spring has earlier peak acceleration and smaller magnitude than a softer spring.

5. Experimental results

This study collects the test data using a real HALT system designed with ED hammers. The current system is unique because it uses ED hammers to produce the input shock pulses to the table instead of the typical pneumatic hammers used by other HALT systems. The hammers are equidistantly arranged from one another around a circular path at the center of the table. Furthermore, the ED hammers together with the controller system were attached in direct contact to the table (Fig. 4).

All hammers are maintained at the same frequency and input power during the test. The table accelerations are measured using two accelerometers (i.e., Acc. 1 and Acc. 2). These accelerations occur on the Z-axis close to Spring 1 and the center of the table.

The time data of the accelerations on the table are analyzed to understand the excitation produced by the HALT machine. The following response data are measured from the locations on the table of a real multi-hammer HALT machine. Two useful methods are further employed to analyze the maximum accelerations in cases using a single hammer and combined multi-hammers (i.e., combinations of Hammers I and II; Hammers I, II, and IV; and Hammers I, II, III, and IV).

(a) k = 4.13 /m

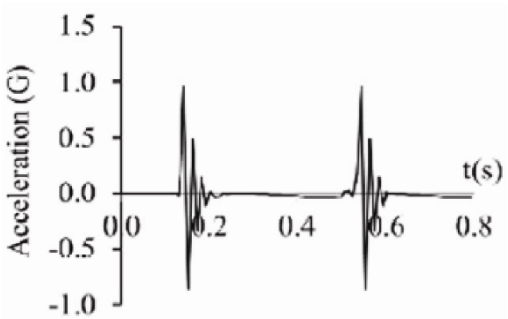

(b) k = 8.26 /m

Fig. 15. Effects of spring stiffness on the accelerations of the table along the Z-axis.

Henderson [16, 17] provided the two best methods to analyze a machine with six degrees of freedom (6-DOF). The first method is shock response spectrum (SRS) based on the high-kurtosis seismic vibration analysis. Biot [18] explored the SRS, while Smithson [19] proposed SRS for 6-DOF machines. The second method uses rainflow analysis to produce a plot known as peak probability distribution function (PPDF) [20].

The SRS is a frequency domain data adopting the time domain peak accelerations and the corresponding natural frequencies of a series of test objects to verify a shock excitation. For example, military standards MIL-STD-810 C, D, and E and other related products prefer the SRS to specify environmental excitation for laboratory simulation. These specifications range from product response to transient and seismic shock. Accordingly, the SRS "fingerprints" such excitations in terms of their stress-related time domain properties [18]. The HALT machine excitations in the current study dynamically occur over periods of seconds. Thus, the SRS is a valuable analysis tool to describe peak amplitudes versus frequency.

The PPDF only measures peak accelerations instead of measuring both the accelerations and instantaneous acceleration history. Although various forms of rainflow analysis exist, the resulting PPDF is a plot of the number of peak occurrences with narrow amplitude ranges. In case of vibration or shock, the PPDF counts the number of acceleration peaks with sigma amplitudes that fall within the defined range bins. A relationship exists between the measured root mean square (RMS) level and the PPDF plot for the current acceleration responses. The RMS value of a signal is equal to a standard deviation

Table 7. Maximum accelerations measured at Spring 1 and at the center of the table when impacted by multiple hammers.

Number of hammers	Hammer	Test number	Maximum acceleration value (G)	
			Acc. 1 (Spring 1)	Acc. 2 (Center of the table)
1	I	1	13.6	2.2
	II	2	9.3	3.0
	III	3	10.9	3.1
	IV	4	25.7	2.7
2	I and II	5	13.6	3.8
	I and III	6	15.1	3.7
	I and IV	7	32.4	2.9
	II and III	8	12.3	3.3
	II and IV	9	25.0	4.1
	III and IV	10	30.8	3.6
3	I, II, and III	11	14.8	4.3
	I, II, and IV	12	38.2	5.5
	II, III, and IV	13	32.7	4.2
	I, III, and IV	14	37.2	4.4
4	I, II, III, and IV	15	32.1	5.2

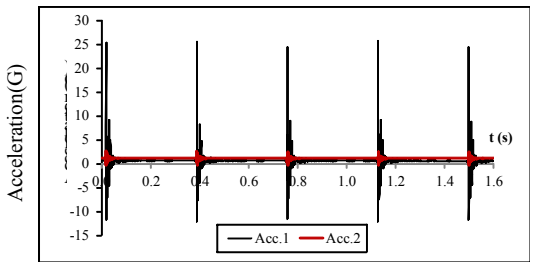

Fig. 16. Time history of accelerations both at Spring 1 measured by Acc. 1 and the center of the table measured by Acc. 2 on a real HALT machine acted upon by Hammer IV.

with a zero mean. The standard deviation is usually represented by a sigma.

Table 7 shows the maximum table accelerations measured near Spring 1 and at the center of the table for the following cases: (1) a single hammer (i.e., Hammers I and II), (2) a combination of two hammers (i.e., Hammers I and II and Hammers I and III), (3) three hammers acting simultaneously (i.e., Hammers I, II, and III), and (4) all four hammers acting simultaneously (i.e., Hammers I, II, III, and IV). The measurement results indicate a significant difference between the acceleration values at the center of the table and at Spring 1. For example, differences are observed between the acceleration values (i.e., 13.6, 9.3, 10.9, and 25.7 G) at Spring 1 when the table is impacted by each of the four hammers. However, only small acceleration variations (i.e., 2.2, 3.0, 3.1, and 2.7 G) occur at the center of the table. Significant differences are also observed between the accelerations at the center of the table and at Spring 1 for all cases. This difference is shown by

taking the time domain signals at the two locations using a continuous 1.6 s measurement (Fig. 16). The case where Hammer IV is directly mounted on the table (Fig. 4) is shown in Fig. 16. The piston inside the hammer immediately rebounds with small accelerations after hitting the anvil at the front end of the hammer. Thus, the magnitudes for each of the instantaneous accelerations are larger on the upper half than those on the lower half (Fig. 16). Furthermore, the directions of the acceleration shock pulses on the table vary from positive to negative (i.e., from approximately +25 G to −10 G).

Using a combination of multiple hammers does not necessarily result in greater impact power. For example, using only three hammers (i.e., I, II, and IV) in Test 14 generates a maximum acceleration of 38.2 G at Spring 1. This acceleration is even higher than that generated by using all four hammers (i.e., I, II, III, and IV; 32.1 G; Table 2).

The PPDF plots with RMS values are shown in Figs. 17(a)-(g). These plots typically originate from the 1.6 s time domain test records on the HALT machine table (Fig. 16). The differences on the RMS values and the number of peaks per second are observed between the cases. Based on the PPDF method, the acceleration effectiveness differs because of the fatigue occurrence on the test specimen for each of the cases using different hammers. The case illustrated in Fig. 17(f) is the most effective because both the highest number of peaks per second and the highest RMS values are achieved. Therefore, using three hammers (i.e., I, II, and IV) provides the best efficiency in the HALT machine.

An SRS plot from the HALT machine table for all foregoing testing cases is shown in Fig. 17(h). Accordingly, the response spectrum magnitudes in all cases are extremely small and without significant difference from each other at low frequencies. The peak accelerations dramatically increase when the repetitive frequency of the hammer increases up to 10 Hz in all cases except those using single hammers (i.e., III and IV). Furthermore, the peaks are observed at around 100 Hz in all cases. These peaks possibly denote the natural frequency of the table. Furthermore, Fig. 17(h) shows that the modal responses of the table are different, that is, they depend not only on the number of hammers in operation but also on the acting position of the hammer.

Another experiment is conducted to examine the effects of changing the swing angle (β) of a hammer. Correspondingly, a cantilever beam that serves as a typical test specimen is attached on top of the table at the Hammer IV position by orienting along the X-axis (Fig. 4). The swing angle β of driving Hammer I varies in two different cases with angles $\beta = 0°$ and $-90°$. The original hammer, which points at the positive X-axis, has a swing angle of $\beta = 0°$. $\beta = -90°$ denotes that the hammer rotates clockwise along its fixed center point with a swing angle of 90° with respect to the positive X-axis (Fig. 13). The table was impacted by a single hammer with the same input setup as the hammer in the two preceding cases. The time history of accelerations at the two measurement positions (i.e., center of the table and beam) is shown in Fig. 19. The accelerations at the center of the table are nearly unchanged under the two different swing angles. By contrast, apparent differences are observed on the beam responses. These differences include peaks at 60 G and 30 G for $\beta = 0°$ and $\beta = -90°$, respectively. The PPDF with RMS for these two cases is also illustrated in Fig. 19. The higher peak number, which focuses on the smaller sigma numbers in the case $\beta = 0°$, denotes the test effectiveness.

6. Summary and conclusions

The table responses to various hammer design combinations in a HALT system determine the effects on the tested products under different impact types. This study examines the problem by initiating a theoretical model that analyzes the impact of a hammer with equivalent spring forces at four table locations, where the springs are mounted. These spring forces are the exerting forces in a subsequent simulation. The piston generates the corresponding impact forces when it moves up and down inside the cylindrical hammer housing. The effects of the impact forces and the spring stiffness on the table motion are also examined theoretically. These theoretical calculations are then verified using a finite element simulation analysis of the HALT system. The satisfactory consistency between the simulation and analytical results reveals that the currently proposed theoretical analysis is correct.

To measure the table accelerations at two specified locations (i.e., near Spring 1 and at the center of the table), the real HALT system in the experiment is impacted by either a single hammer or multiple hammers. The resulting outcomes at these two locations indicate that the theoretical results agree well with the experimental results. Both the PPDF and SRS methods are used to analyze the time domain history of the experimental results. These methods are further utilized to determine how these results could help the HALT system user. For example, Fig. 17(h) provides an overall view of the SRS responses for each of the different combinations of hammers. The PPDF and SRS methods provide the users a better understanding of the appropriate hammers to use in replicating a desired SRS.

Furthermore, the presented methods are proven suitable for solving the HALT system responses. One of the most noteworthy results is the occurrence of the strongest table response accelerations when three hammers are used. Moreover, the experimental data on the SRS plot show the excitation performance in the frequency domain for each of the hammer design combinations. Using three hammers leads to the best frequency domain characteristics, that is, the accelerations are strongest over a wide frequency range. In addition, using a combination of multiple hammers does not necessarily result in higher impact strength. Therefore, one can test products more effectively by choosing a logical combination of multiple hammers. However, users are unable to switch between hammer combinations in the current impact table designs. Thus, the manufacturer should provide design flexibility by

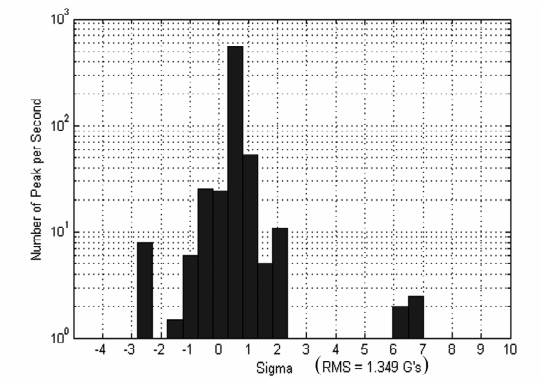

(a) PPDF from data used in Hammer I

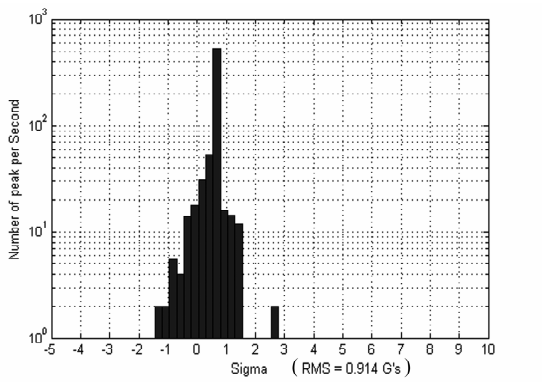

(b) PPDF from data used in Hammer II

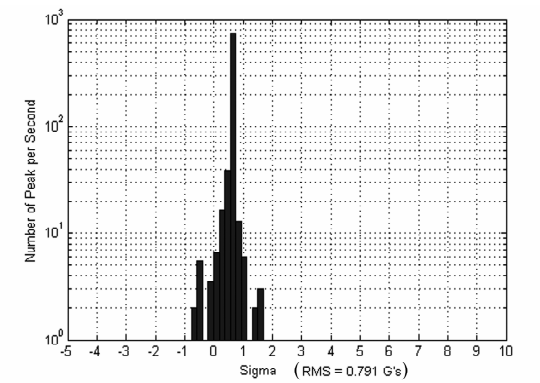

(c) PPDF from data used in Hammer 3

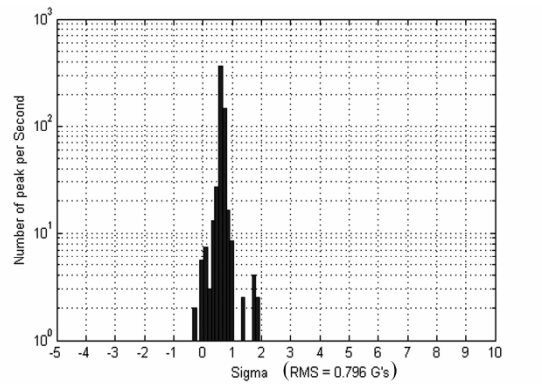

(d) PPDF from data used in Hammer 4

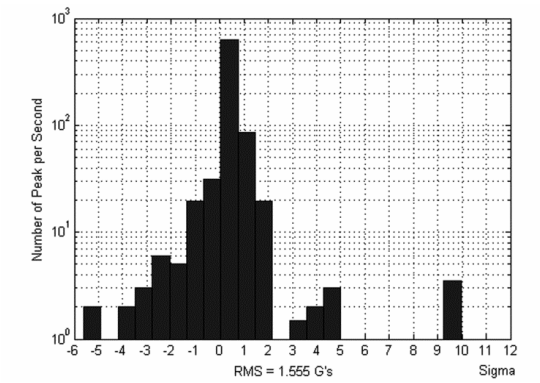

(e) PPDF from data used in Hammers I and II

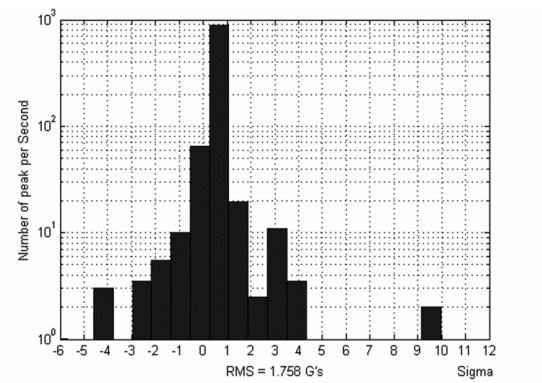

(f) PPDF from data used in Hammers I, II, and IV

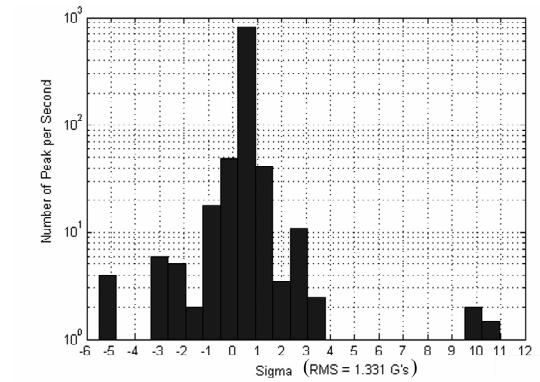

(g) PPDF from data used in Hammers I, II, III, and IV

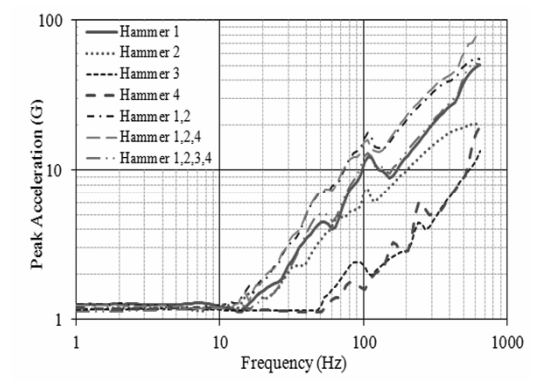

(h) SRS plot of excitations with various hammers

Fig. 17. PPDF and SRS plots for the table responses at Spring 1 for each case using different hammers.

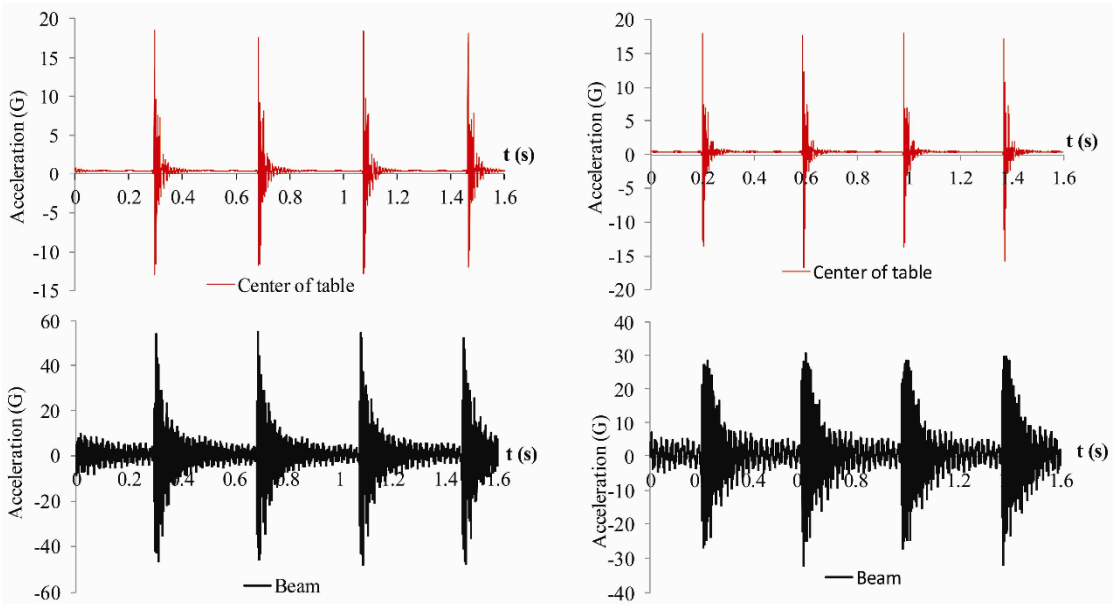

Fig. 18. Time history of accelerations at the center of the table and on a beam acted upon by hammer I with different swing angles.

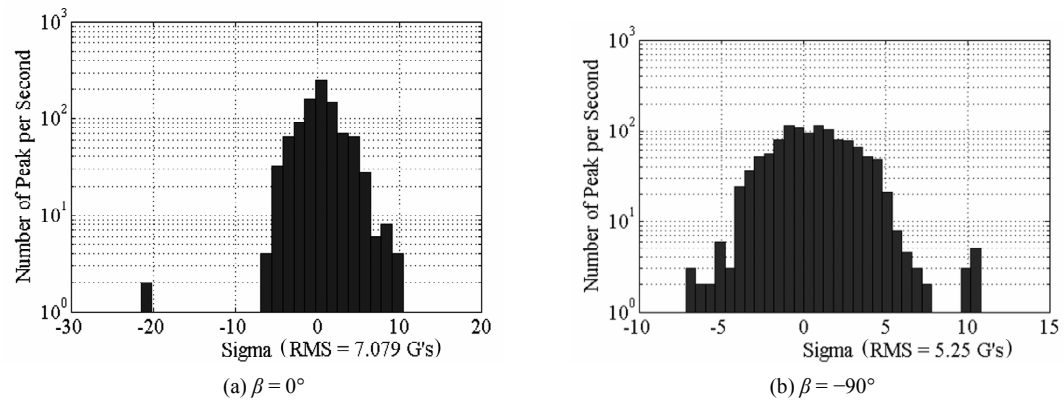

Fig. 19. PPDF from the beam data in Fig. 18.

allowing the users to optionally turn on and off some of the redundant hammers. Waste of resources is avoided by selecting the optimum hammer excitations. Furthermore, the impact forces are better controlled by choosing the appropriate hammer combination.

One design parameter (i.e., how the hammers are mounted on the table with regard to incline angle α and swing angle β) is also important to the response of the table in the HALT system. Changing the spring stiffness also changes the magnitude and shape of the time history shock pulses on the table. The corresponding factor investigations help the designers handle the hardware performances of the machine at the design stage (i.e., before the system is manufactured).

In addition, specific impact types result in different responses at different table locations. This observation has been verified in Sec. 2.3, where the impacts of a single hammer (i.e., Hammer I) are analyzed. This hammer excites different responses at each spring location. Nevertheless, the single hammer has different effects on the table motion at a specific point even at different locations.

One obtains different results (e.g., Tables 3-6) by setting new parameters (i.e., *b*, *c*, *d*, *e*, *E*, and *D*) in the theoretically analyzed formulas (Table 2). The representation of the corresponding force components is simplified at the spring locations along each axis. Thus, recognizing the relationship among these force components and calculating the spring force ratios along all the three axes (i.e., X:Y:Z) are possible. Accordingly, the most efficient test position to mount the specimen on the table of a HALT system becomes apparently achievable. This information is especially beneficial for end users, particularly when deciding on how to mount the test specimen on the table.

Two approaches are used to connect the hammers to a table. One is by directly mounting the hammers under the table, and the other is by leaving a gap between the hammers and the table. The manner by which the hammers are mounted dramatically

changes the shock pulse accelerations on the table. The former results in response pulses with both positive and negative values, whereas the latter results in mostly positive pulses.

Based on all the preceding detailed analyses of the HALT system performances, the future system design can be improved through a user-friendly interface. Such an interface can be created by incorporating the technical information derived from the current study. The interface is then turned into a smart system, which can guide and help the users understand the effects of their chosen settings.

Acknowledgment

The authors express their appreciation for the equipment and funding support provided by King Design Company.

Nomenclature

a : Distance of the springs to the X- and Y-axes
b, c, d, D, e, E, k : Simplified parameters
$\vec{H}(t)$: Exerting force of hammer
$\vec{H}_X, \vec{H}_Y, \vec{H}_Z$: Component forces along the three axes
k_s : Spring stiffness
$\{k_t\}$: Matrix of the total equivalent spring stiffness
r : Distance of the hammers to the center of the table
R : Distance of the springs to the center of the table
$(\vec{S^i M^X})_Z$: Equivalent forces on the springs along the Z-axis
$S^i{}_X, S^i{}_Y, S^i{}_Z$: Component forces on the springs along the three axes
$(\vec{S^i M^Z})$: Force of the spring that generates the moment
$(S^i M^Z)_X$, $(S^i M^Z)_Y$: Component forces on the O-XY plane along the X- and Y-axes
$(S^i T)_X, (S^i T)_Y$: Translational forces located at each spring in the direction of the X- and Y-axes

Greek symbols

α : Incline angle of force $\vec{H}(t)$ to the plane of the table
β : Swing angle between the projection of force $\vec{H}(t)$ on the O-XY plane and the X-axis
δ : Deflection of the spring

Subscripts

i : Spring numbers, i = 1 to 4
X, Y, Z : Direction of the forces along the three axes

References

[1] H. J. Yuan and T. M. Jiang, Characteristics of Omni-Axes Random Vibration Environment and Its Stimulation Effect, *Structure & Environment Engineering*, 33 (2) (2006) 1-5.

[2] F. F. Wang, Modified highly accelerated life test for aerospace electronics, *Thermo-mechanical Phenomena in Electronic Systems, Proceedings of the Intersociety Conference*, Lunnwood, WA., USA (2002) 940-945.

[3] G. K. Hobbs, What HALT and HASS can do for your products, *Evaluation Engineering*, 36 (11) (1997) 138-143.

[4] H. S. Liu, Environmental stress screening equipment: search, evaluation, design, experimentation, *Test Engineering and Management* (1994)10-14.

[5] H. S. Liu, New approach for production line Environmental Stress Screening, *Test Engineering and Management*, 67 (4) (2005) 18-19.

[6] Li Xiao-Yang, Jiang Tong-Min and Zhang Wei, A multi-axis vibration fixture based on electromagnetic shaker, *Proceedings of the IEEE 8th Reliability, Maintainability and Safety,* Chengdu, China (2009) 1183-1186.

[7] D. Lee, J. Zhuge, Y. C. Chuang and Y. S. Chen, Comparing features of the newly developed electrodynamic hammer and the general pneumatic hammer used in environmental stress screening systems, *Proceeding of the Institute of Environmental Sciences and Technology Conference*, Florida, USA (2012) 453-465.

[8] B. B. Muvdi, A. W. Al-Khafaji and J. W. McNabb, Equilibrium of rigid bodies in three dimensions, *Statics for Engineers*, Springer-Verlag, New York, USA (1997) 228-307.

[9] H. R. Harrison and T. Nettleton, Force systems and equilibrium, *Principles of Engineering Mechanics*, 2nd ed., Butterworth-Heinemann, London, U.K. (1994) 37-53.

[10] J. L. Meriam and L. G. Kraige, Force systems, *Engineering Mechanics*, *SI Version: Statics*, 6th ed., John Wiley & Sons Inc., New Jersey, USA (2008) 23-50.

[11] R. K. Vierck, *Vibration analysis*, 2nd ed., Crowell Company, New York, USA (1979).

[12] S. Rajasekaran and G. Sankarasubramanian, Fundamental concepts of structures, *Computational Structural Mechanics*, Prentice-Hall, New Delhi, India (2001) 60-62.

[13] Mario Paz and W. E. Leigh, Undammed single degree-of-freedom system, *Structural dynamics Theory and Computation updated with SAP2000*, 5th ed., Kluwer Academic publishers, Massachusetts, USA (2004) 7-8.

[14] Thomas D. Rossing and Neville H. Letcher, Free and force vibration of simple system, *Principles of Vibration and Sound*, 2nd ed., Springer-Verlag, New York, USA (2004) 15-17.

[15] S. Graham Kelly, Modeling of SDOF system, *Mechanical Vibrations: Theory and Applications*, SI Edition, 1st ed., Cengage Learning Inc., Connecticut, USA (2012) 62-67.

[16] G. Henderson, 6DOF machine characteristics and method of measuring effectiveness, *Test Engineering & Management* (1992) 10-12.

[17] G. Henderson, *Dynamic characteristics of repetitive shock machine*, GHI Systems Incorporated, San Pedro, California, USA (1993).

[18] M. A Biot, Theory of elastic system vibration response under transient excitation with an application to earth quake resistant building, *Journal of Applied Sciences,* 19 (1933) 260-268.

[19] Smithson, Stephen A, Shock response spectrum analysis for ESS and STRIFE/HALT measurement*, Proceedings, IES*, San Diego, California, USA (1991).

[20] N. E. Dowling, Fatigue failure predictions for complicated stress-strain histories, *Journal of Materials*, 7 (1) (1972) 1-17.

Y. S. Chen is an Associate Professor at the Department of Mechanical Engi - neering, Yuan-Ze University, Taoyuan, Taiwan. He received his Ph.D. in mechanical engineering from the University of Maryland, College Park. He has worked closely with the industry in areas related to the mechanical reliability assessment of electronic products, including vibration analysis, structural analysis, packaging design, and material properties investigation.

Le Hong Chuong received his B.S. and M.S. degrees in Mechanical Engineering from the National University of Civil Engineering, Vietnam, in 2000 and 2006, respectively. He is currently pursuing his Ph.D. at the Department of Mechanical Engineering, Yuan-Ze University, Taiwan. His current research interests include electronic packaging analysis, computer-aided engineering analysis, mechanical system design, and automotive engineering.